Biochimica et Biophysica Acta 1853 (2015) 1980–1991

Contents lists available at ScienceDirect

Biochimica et Biophysica Acta

journal homepage: www.elsevier.com/locate/bbamcr

Review

Structural insights into endoplasmic reticulum stored calcium regulation by inositol 1,4,5-trisphosphate and ryanodine receptors☆

Min-Duk Seo [a,b,1], Masahiro Enomoto [c,1], Noboru Ishiyama [c,1], Peter B. Stathopulos [d,1], Mitsuhiko Ikura [c,*]

[a] Department of Molecular Science and Technology, Ajou University, Suwon, Gyeonggi 443-749, Republic of Korea
[b] College of Pharmacy, Ajou University, Suwon, Gyeonggi 443-749, Republic of Korea
[c] Princess Margaret Cancer Centre, University Health Network, University of Toronto, Toronto, ON M5G 1L7, Canada
[d] Department of Physiology and Pharmacology, Schulich School of Medicine and Dentistry, University of Western Ontario, London, ON N6A 5C1, Canada

ARTICLE INFO

Article history:
Received 11 October 2014
Received in revised form 17 November 2014
Accepted 19 November 2014
Available online 25 November 2014

Keywords:
Calcium signaling
Calcium release channel
Inositol 1,4,5-trisphosphate receptor (IP_3R)
Ryanodine receptor (RyR)
Protein structure
X-ray crystallography
Nuclear magnetic resonance (NMR)
Electron microscopy (EM)

ABSTRACT

The two major calcium (Ca^{2+}) release channels on the sarco/endoplasmic reticulum (SR/ER) are inositol 1,4,5-trisphosphate and ryanodine receptors (IP_3Rs and RyRs). They play versatile roles in essential cell signaling processes, and abnormalities of these channels are associated with a variety of diseases. Structural information on IP_3Rs and RyRs determined using multiple techniques including X-ray crystallography, nuclear magnetic resonance (NMR) spectroscopy and cryo-electron microscopy (EM), has significantly advanced our understanding of the mechanisms by which these Ca^{2+} release channels function under normal and pathophysiological circumstances. In this review, structural advances on the understanding of the mechanisms of IP_3R and RyR function and dysfunction are summarized. This article is part of a Special Issue entitled: 13th European Symposium on Calcium.

1. Importance of calcium signaling by sarco/endoplasmic calcium release channels

1.1. Critical roles of IP_3Rs and RyRs for the normal cell functions

As a small and non-degradable intracellular messenger, the calcium ion (Ca^{2+}) is responsible for directing numerous intracellular signaling pathways [1–3]. The versatility of Ca^{2+} signaling occurs *via* the modulation of amplitude, duration and spatio-temporal patterning, enabling the control of diverse and kinetically distinct cellular processes including for example, cell proliferation, cell migration, gene transcription and initiation of cell-death pathways [4, 5]. This versatility emerges from a wide repertoire of signaling proteins called the Ca^{2+} signaling toolkit [4, 5] which together orchestrate communicative changes in compartmentalized Ca^{2+} levels. There are two classes of Ca^{2+} handling macromolecules on the SR/ER membrane: 1) Ca^{2+} release channels that liberate internally stored Ca^{2+} into the cytoplasm, and 2) Ca^{2+} pumps that move cytosolic Ca^{2+} back into the SR/ER. The release of Ca^{2+} from the SR/ER occurs at minimal energy expenditure due to the high Ca^{2+} concentration gradient maintained between the cytosol and SR/ER lumen (*i.e.* cytosolic Ca^{2+} ~0.1–1 μM *versus* SR/ER luminal Ca^{2+} ~1 mM), while refilling of the SR/ER lumen is an energy demanding process.

The two major families of Ca^{2+} release channels include the inositol 1,4,5-trisphosphate receptors (IP_3Rs) and the ryanodine receptors (RyRs). Molecular characterization of IP_3Rs and RyRs has dramatically improved our understanding of the bases for the regulation of SR/ER Ca^{2+} signaling processes [6,7]. The IP_3Rs and RyRs are transmembrane protein cousins with similar functional characteristics. Although IP_3Rs absolutely require inositol 1,4,5-trisphosphate (IP_3) for activation, they can be considered Ca^{2+}-induced Ca^{2+} release channels akin to RyRs, since both IP_3R and RyR require low Ca^{2+} levels for channel activation and are inactivated at high Ca^{2+} levels [8–10]. Three isoforms of IP_3Rs (IP_3R1, IP_3R2, and IP_3R3) and RyRs (RyR1, RyR2, and RyR3) have been identified in mammalian vertebrates [11]. In non-mammalian vertebrates three isoforms of IP_3Rs and two RyR isoforms (RyRα and RyRβ) have been discovered [12, 13]. Remarkably, recent structural elucidation of IP_3Rs and RyRs revealed an analogous tetrameric overall architecture and striking similarity in the activation mechanisms of these channels (see below). Here, we review the structural properties of these channels focusing on state-of-the-art X-ray crystallography, nuclear magnetic

☆ This article is part of a Special Issue entitled: 13th European Symposium on Calcium.

* Corresponding author at: Room 4-804, TMDT, MaRS Centre, 101 College Street, Toronto, ON M5G 1L7, Canada. Tel.: +1 416 581 7550; fax: +1 416 581 7564.
E-mail address: mikura@uhnres.utoronto.ca (M. Ikura).

[1] Contributed equally to this work.

http://dx.doi.org/10.1016/j.bbamcr.2014.11.023
0167-4889/

resonance (NMR) spectroscopy and cryo-electron microscopy (EM) data that have revealed crucial functional mechanisms for these proteins.

1.2. IP_3R related diseases

The roles of IP_3Rs have been shown for ataxia, heart disease, exocrine secretion deficit, taste perception deficit, several cancers and neurodegenerative diseases such as Alzheimer's disease (AD) and Huntington's disease (HD) to name a few [14–23]. In this review we focus on several cancers, AD and HD. In cancer cells, Ca^{2+} signaling mechanisms are frequently remodeled or deregulated [21,23,24]. Although alterations in Ca^{2+} signaling may not be a requirement for the initiation of cancer, altered Ca^{2+} mobilization has been observed in breast and other cancer cells, and known to contribute to tumor progression [21,23,25,26]. Currently little is known about what specific players in the Ca^{2+} signaling tool kit contribute to the altered Ca^{2+} mobilization in cancer cells and how Ca^{2+} signaling cross-talks with well-known cancer pathways such as the Ras/Raf/MAPK pathway [27]. However, increasing numbers of studies indicate the relevance of IP_3Rs to cancer. Type 1 IP_3R (*i.e.* IP_3R1) expression is reduced and type 3 IP_3R (*i.e.* IP_3R3) expression is increased in human glioblastoma tissues, compared to normal human brain [28]. Specific inhibition of IP_3R3 by caffeine reduces the migration, invasion and survival of glioblastoma cells [28]. Increased IP_3R3 levels are also observed in colorectal cancer [29]. Furthermore, multiple B-cell lymphoma 2 (Bcl-2) family proteins, which have pro- and anti-apoptotic functions, directly bind to different sites on IP_3Rs and elicit various effects on IP_3R function [30–33], suggesting that IP_3R is an important hub for the action of Bcl-2 family proteins in various physiological and pathological settings including tumor progression. Interestingly, a recent paper has linked the Ras signaling pathway, which is frequently deregulated in cancer [34], to the IP_3R Ca^{2+} release pathway. By comparing the parental human colorectal cancer cell line harboring the K-Ras mutant allele (G13D) to an isogenic derivative in which the mutated K-Ras allele is deleted, it was demonstrated that oncogenic K-Ras inhibits IP_3-induced Ca^{2+} release (IICR) from the ER through remodeling of IP_3R isoform composition [35]. Very recently, a progressive study demonstrated a closer link between K-Ras and IP_3R showing that K-Ras4B is translocated from the plasma membrane to ER upon phosphorylation of serine 181 (S181) by protein kinase C (PKC) [36]. The translocated GTP-bound active form of K-Ras4B forms a ternary complex with IP_3R and Bcl-xL and promotes cell death [36], indicating that IP_3R is a novel effector of K-Ras4B.

Two common hallmarks of AD and HD are the aggregation of misfolded proteins and dysregulated Ca^{2+} homeostasis [14,15]. Exaggerated IP_3R-mediated Ca^{2+} release from ER has been reported in non-neuronal cells from pre-symptomatic familial AD (FAD) patients, neurons in AD mouse models and *Xenopus oocytes* expressing presenilin 1 and 2 mutants [17,37–40]. The mechanism of the exaggerated Ca^{2+} release *via* IP_3R is not fully understood. One model is that FAD mutations in presenilins cause elevated ER Ca^{2+} levels, resulting in enhancement of IP_3R-mediated Ca^{2+} release [41–43]. Another hypothesis is that the direct interaction of mutant presenilins with IP_3R enhances Ca^{2+} release activity of IP_3R [44, 45]. Further studies will be needed for a deeper understanding of the dysregulation of IP_3R in the AD pathogenesis. HD is an autosomal-dominant neurodegenerative disorder caused by polyglutamine expansion in the amino-terminus of huntingtin (Htt) [46]. It is well known that mutant Htt (mHtt) acquires toxic gain of functions [47]. The direct interaction of mHtt with the C-terminal region of IP_3R1 was first reported in 2003 [48]. The affinity of mHtt to IP_3R1 increases when mHtt is associated with huntingtin-associated protein 1A (HAP1A) [48]. Moreover, mHtt, but not normal Htt, sensitizes IP_3R1 activity in planar lipid bilayers [48]. Later, this direct interaction was confirmed using an unbiased high-throughput screening assay [49]. Recently, it was discovered that the direct interaction of IP_3R1 with ER stress chaperone protein GRP78 is impaired in HD R6/2 model mice, resulting in the dysregulation of IP_3R1 signaling [50]. This line of studies strongly suggests a role for IP_3R in the HD pathogenesis.

1.3. RyR related diseases

Several cardiac and skeletal muscle disorders are associated with hundreds of different RyR mutations. Most disease-associated mutations are clustered in three regions on RyRs: 1) the N-terminal region (*i.e.* residue range ~1–600), 2) the central region (*i.e.* residue range ~2100–2500) and 3) the C-terminal region (residue range ~3900–5000). Mutations in RyR1, which are mainly found in the skeletal muscle [51], have been associated with malignant hyperthermia (MH) [52–55], central core disease (CCD) [56–58] and multiminicore disease [59]. In RyR1, most MH mutations are located on the N-terminal and central regions, whereas the mutations causing CCD are found in the C-terminal region [60]. MH is characterized by increased temperature, heart rate and rigidification of the muscles usually triggered by the combination of RyR1 mutations and an exposure to drugs such as volatile anesthetic agents [61]. Dantrolene is clinically used to treat MH, and while the molecular action mechanism of dantrolene remains elusive, it is known that dantrolene decreases intracellular Ca^{2+} concentrations by inhibiting RyR1 in the SR membrane [62–64].

RyR2 is predominantly expressed in cardiac myocytes [65,66], and mutations in RyR2 have been linked to catecholaminergic polymorphic ventricular tachycardia (CPVT) and arrhythmogenic right ventricular dysplasia (ARVD) [67]. In cardiac muscle cells, RyR2 is activated when luminal Ca^{2+} levels increase to a certain threshold, which is termed store overload-induced Ca^{2+} release (SOICR); disease-associated mutations in RyR2 may lower the SOICR threshold [68, 69]. However, the precise molecular mechanisms that drive luminal Ca^{2+} sensing have been elusive. Recently, it was proposed that the helix bundle crossing region of RyR2 (*i.e.* the RyR2 gate) located in the predicted C-terminal inner helix of RyR2 directly senses the luminal Ca^{2+} store, and residue E4872 is essential for this sensing [70]. Consistent with this notion, a single mutation (*i.e.* E4872A or E4782Q) in RyR2 completely abolished luminal Ca^{2+} activation. Pharmacologically, therapeutic agents reducing RyR2 open time suppress Ca^{2+}-triggered ventricular tachycardias (VTs) [71–73]. Mouse hearts harboring an E4872Q mutation were also shown to be protected against Ca^{2+}-triggered VT by reducing RyR2 open time [70]. Therefore, the 'RyR2 gate' could be a potential target for anti-arrhythmic therapeutics. Finally, although no disease-associated mutations have been identified in RyR3 thus far, recent studies suggest that RyR3 is related to neurodegenerative diseases such as Alzheimer's disease [74,75].

It is not surprising that, as the key Ca^{2+} signaling regulators in various tissues, both IP_3R and RyR are implicated in human disease. To understand how the malfunction of IP_3R and RyR leads to different abnormalities in humans, we ought to elucidate the structure and function relationship of those key players in Ca^{2+} signaling. In the past 15 years, significant progress has been made in our understanding of the three-dimensional structure of IP_3R and RyR, despite the large molecular size. Below we will overview the 'past and present' of the structural studies of the two important molecules in Ca^{2+} signaling.

2. High-resolution structures of IP_3Rs and RyRs

2.1. The N-terminal domains of IP_3Rs

At present, seven structural fragments of IP_3Rs have been determined by X-ray crystallography, and all the structures cover the N-terminal region (NT) of IP_3Rs [76–79]. The NT of IP_3Rs contains two functional domains: 1) the suppressor domain (SD) and 2) the IP_3-binding core (IBC); together these domains bind IP_3 and initiate channel channel gating (Fig. 1A). Interestingly, the IBC is the minimal region required for IP_3 binding, and IBC alone can bind to IP_3 with extremely high affinity; however, the IP_3-binding affinity of the entire NT encompassing both the SD

and IBC is reduced more than twenty times, suggesting that the SD inhibits the IP_3 binding to the IBC [80]. In addition to the suppressive role of the SD, it is essential for IP_3-induced channel gating, as a single mutation within the SD (*i.e.* Y167) abolishes IP_3-evoked Ca^{2+} release without affecting the IP_3 binding affinity [81]. Although the exact mechanism how the IP_3-binding induced signals are transmitted to the channel domain remains elusive, the critical loop in the SD containing Y167 is essential for linking IP_3 binding to channel gating.

The first high-resolution structure of IP_3Rs was the IBC of IP_3R1 (*i.e.* residues 224–604) in complex with IP_3 (*i.e.* PDB code 1N4K) [76]. The IBC contains a β-domain (IBC-β) and α-domain (IBC-α), adopting a β-trefoil fold and an armadillo repeat fold, respectively (Fig. 1B). The two domains are located almost perpendicular to each other, forming an L-shaped structure of IBC. The cleft between IBC-β and IBC-α creates the IP_3 binding site. The crystal structure of the SD for IP_3R1 (*i.e.* residues 1–223; PDB code 1XZZ) [77] is nearly identical to that for IP_3R3 (*i.e.* residues 1–224; PDB code 3JRR) [81]. The SD forms a hammer-like structure with 'head' and 'arm' subdomains. The 'head' subdomain of the SD adopts a β-trefoil fold similar to IBC-β, and the 'arm' subdomain of the SD consists of a helix-turn-helix conformation. However, the IP_3R1-SD and IP_3R3-SD show different molecular surface properties which may contribute to isoform-specific differences in IP_3-binding affinity [82] (Fig. 1C).

Recently, two research groups independently determined crystal structures of the NT of IP_3R1 (*i.e.* residues 1–604). Lin et al. solved both apo- and IP_3-bound NT structures of rat IP_3R1 at 3.8 Å resolution from a single crystal grown in the presence of IP_3 (*i.e.* PDB code 3T8S) [79]. Subsequently, the NT structures of rat IP_3R1 with all Cys residues mutated to Ala (*i.e.* Cys-less form) at higher resolutions have been determined. Importantly, the crystals were separately grown in the absence and presence of IP_3, and apo- and IP_3-bound NT structures were resolved to 3.0 Å for the apo-state (*i.e.* PDB code 3UJ4) and 3.6 Å for IP_3-bound state (*i.e.* PDB code 3UJ0) (Fig. 1D) [78]. The SD, IBC-β and IBC-α in the NT structure form a triangular architecture with the SD positioned behind the IP_3-binding site. This arrangement suggests that the SD allosterically inhibits the IP_3 binding. Specifically, the SD interacts with IBC-β and IBC-α, forming two discrete interfaces (*i.e.* β-interface and α-interface). Hydrophobic interactions dominate the short β-interface, stabilized by a salt bridge. The longer α-interface consists of both hydrophobic and electrostatic interactions (Fig. 1D), and plays an essential role in the inhibitory effects of the SD on IP_3 binding [78]. The structural comparison of NTs in the absence and presence of IP_3 reveals the IP_3 binding-induced conformational changes that are essential for channel activation. The most significant structural change by IP_3 binding is the domain reorientation between IBC-β and IBC-α, resulting in partial closure of the IP_3-binding cleft (Fig. 1E). Surprisingly, the hydrophobic and electrostatic interactions forming the α-interface are completely maintained after IP_3 binding, while the β-interface is disrupted resulting in a slight increase in the distance between the SD and IBC-β. Additionally, the SD rotates towards the IBC, and the direction of swing is nearly perpendicular to the closure of IBC. Ultimately, the IP_3-evoked conformational changes within NT cause the movement of the critical loop in SD, especially the Y167 position, probably coupling the SD reorientation to the activation of the channel domain [78,81].

2.2. The N-terminal and phosphorylation domains of RyRs

The first high-resolution structures of RyR determined by X-ray crystallography were of the first ~210 residues making up the N-terminal region (*i.e.* A domain) of RyR1 (*i.e.* PDB codes 3HSM and 3ILA) [83,84] and RyR2 (*i.e.* PDB code 3IM5) [84], elucidating that the A domain folds into β-trefoil core consisting of twelve β-strands and a single α-helix (Fig. 1F). These initial structures revealed that a high frequency of disease-related mutations for RyR1 (*i.e.* MH and CCD) and RyR2 (*i.e.* CPVT and ARVD) cluster in and around the loop connecting β8 and β9, termed the hot spot (HS) loop [83,84]. Recently, a mutant of the RyR2-A associated with a severe form of CPVT has been investigated [85]. The mutant consists of a deletion encompassing the entire third exon of RyR2 encoding a 35-residue stretch made up of a β-strand and an α-helix. Remarkably, rather than marked destabilization and misfolding of this deletion mutant, the structural fold of the RyR2-A is maintained by the insertion of a flexible loop that is located immediately downstream of the deletion into the β-trefoil core (Fig. 1G; see also Section 4).

The crystal structure of the larger N-terminal region (*i.e.* residues 1–559) of RyR1 has been successfully determined (*i.e.* PDB code 2XOA) [86]. This larger construct encompasses three domains termed A, B and C (Fig. 1A). Domains A and B fold into β-trefoil cores and domain C is composed of a five-helix bundle (Fig. 1H). These three domains interact with each other primarily *via* hydrophobic interactions, and 56 different disease-associated mutations from RyR1 and RyR2 are mapped onto this structure [86]. To our surprise, the domain architecture found in RyR1 is essentially identical to that previously reported for IP_3R, despite the low sequence similarity between the two proteins (17% identity). More recently, the same group solved the crystal structures of 8 mutants of the RyR1-ABC that affect intra-subunit domain–domain interfaces [87]. The location of these mutations and their impact on RyR structure and function are discussed in Section 3 of this review.

The first crystal structures outside the N-terminal region of RyR have been independently solved by two groups [88,89]. The phosphorylation domains from rabbit RyR1 (*i.e.* residues 2734–2940; PDB codes 4ERT and 3RQR) [88,89], mouse RyR2 (*i.e.* residues 2699–2904; PDB code 4ETV) [89], human RyR3 (*i.e.* residues 2597–2800; PDB code 4ERV) [89] and several disease-associated mutants [89] were determined from 1.6 to 2.2 Å. In both RyR1 and RyR2, the domain consists of a two-fold symmetrical structure in which each half is composed of two α-helices, one or more short 3_{10} helices and a C-terminal β-strand (Fig. 1I). These symmetrical repeats are separated by a long and flexible loop (Fig. 1I), which contains the previously identified phosphorylation target residues S2834 in RyR1 and S2808/S2814 in RyR2. The two halves interact with one another with the β-strands forming a short antiparallel β-sheet. In the corresponding domain of RyR3 the overall symmetry is less conserved, where the flexible loop is partially replaced by an additional α-helix.

3. Combination of X-ray crystallography and EM

Because of the large molecular size of IP_3R and RyR, successful structure determination was made possible for relative small domains in

Fig. 1. (A) Domain architecture for IP_3R1 and RyR1. The numbers on top of the domain diagram represent the amino acid residues of rat IP_3R1 and rabbit RyR1. (B) Structure of the IBC in complex with IP_3 (PDB code 1N4K). Cartoon representation of the IBC-β (light green) and IBC-α (orange) are shown, and the IP_3-coordinating residues are colored red. (C) Electrostatic surface of the SD from IP_3R1 (PDB code 1XZZ) and IP_3R3 (PDB code 3JRR). The acidic pocket in IP_3R3-SD and the equivalent region in IP_3R1-SD are highlighted (white circle). (D) Superposed apo-NT (SD, blue; IBC-β, green; IBC-α, yellow, PDB code 3UJ4) and IP_3-bound NT (magenta, PDB code 3UJ0) structures by overlaying the IBC-β. The side chains of Y167 in apo-NT and IP_3-bound NT are depicted as sticks in square with dotted line. Close-up view of the α-interfaces in the apo- and IP_3-bound states is also depicted (square with dotted line). Residues forming the interface are represented by sticks. (E) IP_3-induced conformational change in the IBC is depicted with the same color code as panel (C). The black lettering and red lettering (α11 and α12) represent the α-helices in apo-NT and IP_3-bound NT, respectively. (F) Cartoon representation of wild-type RyR2-A (PDB code 3IM5). HS loop is colored magenta. Exon 3 is shown as orange, and the flexible loop replacing exon 3 in the RyR2-A delta exon3 structure is indicated by a red dotted line. Side chains of disease-associated mutations are colored gray. (G) Cartoon representation of RyR2-A delta exon3 (PDB code 3QR5). The rescue segment is shown in red. (H) Cartoon representation of RyR1-ABC (PDB code 2XOA). Side chains of disease-associated mutations located on inter-subunit interfaces and intra-subunit interfaces (or buried) are colored red and blue, respectively. (I) Cartoon representation of RyR1 phosphorylation domain (PDB code 4ERT). The two halves of two-fold symmetrical structure are shown in different colors (blue and yellow). Flexible phosphorylation loop is indicated by a black dotted line, and the position of the well-studied phosphorylation site S2843 is indicated. Side chains of disease-associated mutations are colored gray.

those proteins. This 'divide-and-conquer' approach has been used for many protein structure determinations in the past, proven to be extremely powerful in the field of structural biology. However, both IP_3R and RyR are a tetrameric transmembrane protein, and hence full understanding of their structure–function relationships has to involve the elucidation of the tetrameric structures. Recent EM studies on full-length proteins, combined with both X-ray and NMR structures of NT domains, have dramatically improved our understanding of the tetrameric receptors. We will discuss below the outcome of the EM structure determination of IP_3R and RyR.

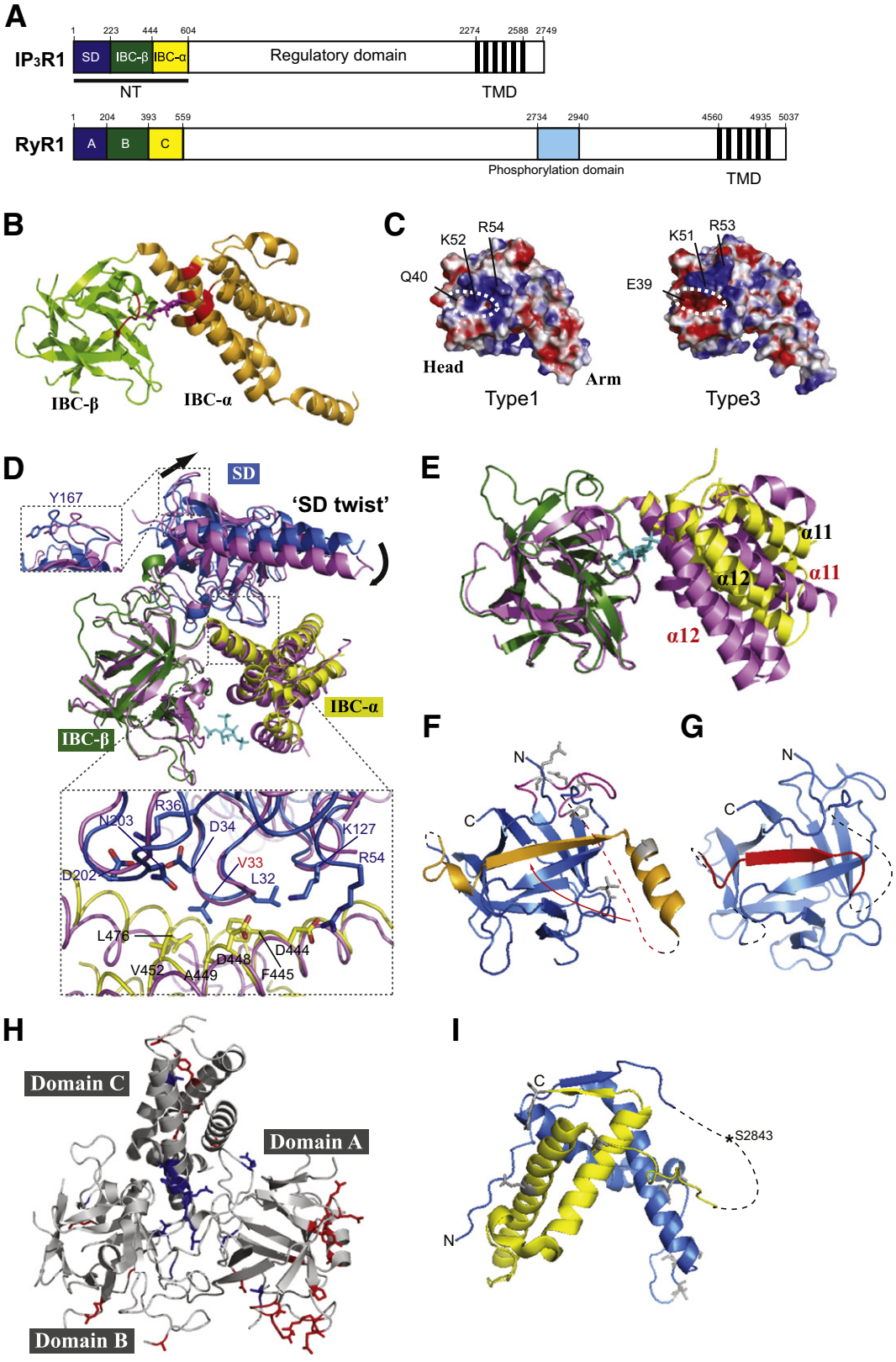

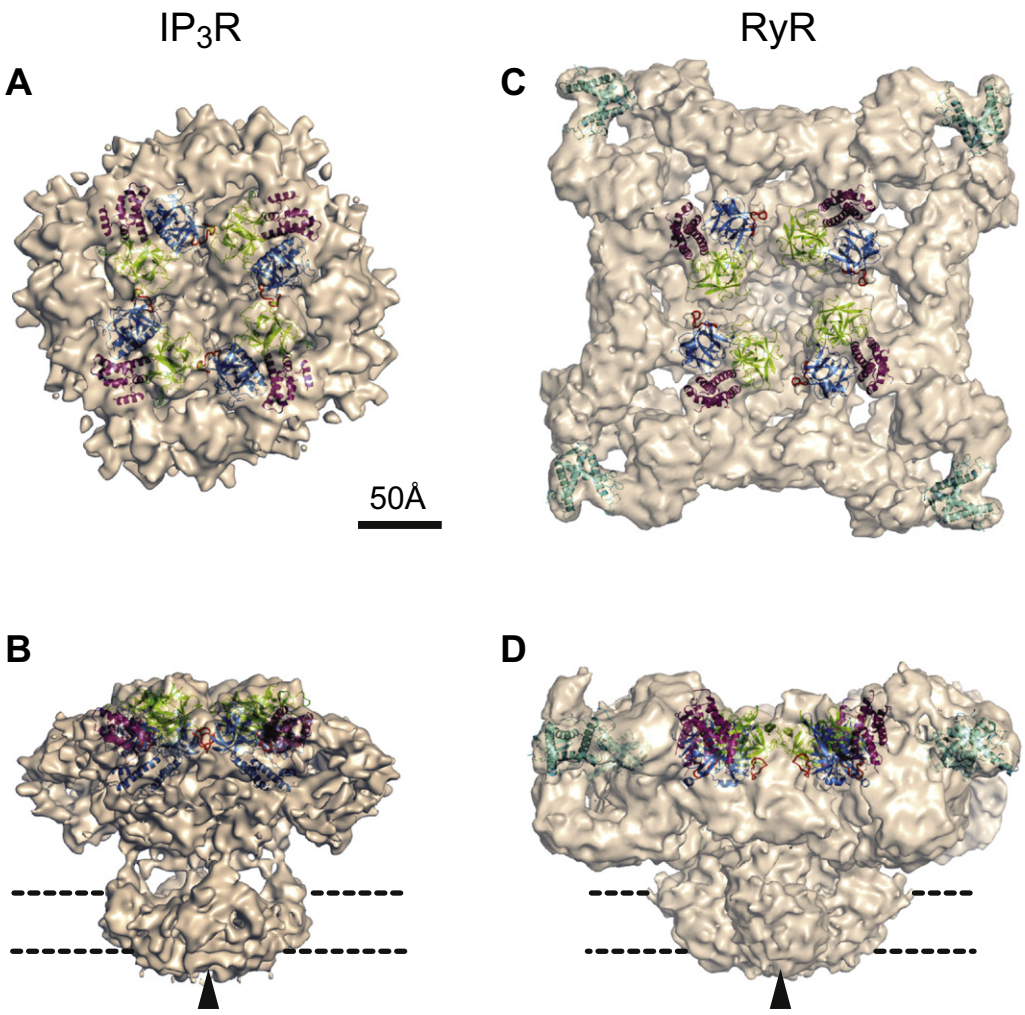

Fig. 2. Quasi-atomic models of IP_3R and RyR tetramers. Cryo-EM structures of IP_3R1 (A, B) (EMDB code 5278) and RyR1 (C, D) (EMDB code 1275) in the closed state are shown from top (A, C) and side (B, D) views. Crystal structures of IP_3R1-NT (PDB code 3UJ0), RyR1-ABC (PDB code 2XOA) and RyR-phosphorylation domains (PDB code 3RQR) are shown as ribbon representation (SD and A domains in blue, IBC-β and B domains in green, IBC-α and C domains in purple and RyR-phosphorylation domain in teal). The hotspot loops in RyR1-A and IP_3R1-SD domains are indicated by red loops. The luminal side of the ion conduction pore is indicated by arrow heads (B, D). Membrane bilayer is depicted as dotted lines.

3.1. EM structures of IP_3R and RyR

While several crystal structures of IP_3R and RyR fragments have now emerged, a major task remains in piecing together these fragments into full-length structures. To facilitate this effort, IP_3R purified from rat cerebellum [90] and RyR purified from rabbit skeletal muscle [91] were frozen in vitreous ice and analyzed by single-particle cryo-EM. Cryo-EM maps of RyR1 have been determined by a number of laboratories [92, 93], and have consistently indicated that the full-length RyR tetramer has a mushroom-like appearance with an enormous cytoplasmic region sitting on top of a transmembrane domain (Fig. 2). The highest resolution cryo-EM map of RyR in a closed conformation was initially reported at 9.6 Å [92], but later revised to be 12 Å based on adopting the "gold-standard" approach [94]. Samso et al. also determined cryo-EM structures of RyR at lower resolution in the open- and closed-channel states, suggesting that channel activity is likely linked to allosteric conformational changes within the full-length structure [93]. Recently, new cryo-EM structures of RyR1 with higher resolutions (up to 4.8 Å) were deposited in the Electron Microscopy Data Bank (EMDB codes 2751, 2752, 6106 and 6107).

In contrast, previously determined cryo-EM maps of IP_3R have revealed various shapes with little resemblance to each other. These inconsistencies are likely due to inherent flexibility and heterogeneity of samples prepared by the different research groups. Nonetheless, a cryo-EM map of the IP_3R tetramer in a closed conformation was obtained by Ludtke et al. in 2011 [95], and its relevance was confirmed through numerous methods including tilt-pair validation [96]. This cryo-EM structure revealed a height for IP_3R of ~160 Å, nearly identical to RyR with a smaller cytoplasmic region resting on the transmembrane domain (Fig. 2). The resolution of the IP_3R structure was initially reported as 10 Å, but was revaluated to be 14–17 Å [96], partly due to higher variances detected in the internal architecture of the cytoplasmic region compared to the solvent-exposed exterior and transmembrane regions.

3.2. Docking of crystal structures onto EM maps

Determination of cryo-EM maps of IP_3R and RyR at a nanometer-level resolution has provided opportunities to perform rigid-body docking of crystal structures of the IP_3R and RyR fragments in order to produce quasi fully-assembled models. Computational docking programs, such as SITUS [97], were used to position IP_3R1-NT [78] and RyR1-ABC [86] near the top of their respective mushroom-shaped cytoplasmic structures, with the 'arm'-motifs of IP_3R1-SD and RyR1-A pointing towards the inner core of the structure (Fig. 2A). Interestingly,

the asymmetric shapes of the RyR1-ABC domains allowed the individual domains, RyR-A, -B and -C, to be independently docked into the same positions [86]; however, similar attempts to fit the smaller RyR-phosphorylation domains resulted in ambiguous positions within the clamp region (Fig. 2C, D) [88,89]. For both IP_3R and RyR, four NT/ABC molecules form a ring around the four-fold symmetry axis of the full-length structures [78,86]. These quaternary arrangements suggest that the 'hot-spot' loop of RyR-A [83] and the equivalent loop of IP_3R-SD are involved in creating the inter-subunit interfaces by interacting with flexible loops of RyR-B and IP_3R-IBC-β from adjacent subunits, respectively.

Comparison of quasi-atomic models of IP_3R and RyR produced from combining crystal structures and cryo-EM maps have revealed structural and functional similarities between the two channels. First, although the cytoplasmic region of RyR is considerably larger than IP_3R, the relative positions of N-terminal NT/ABC regions are virtually identical with respect to the location of the transmembrane channel regions of these receptors [78]. This is likely a reflection of crucial roles played by the N-terminal region and transmembrane domain in forming functional tetramers of IP_3R and RyR, likely through a common mechanism. It is noteworthy that the ability of the isolated NT regions of IP_3R and RyR1, 2 and 3 to oligomerize has been recently demonstrated [98–100]. Remarkably, it was also shown that the RyR-A could be functionally substituted with the IP_3R-SD and the transmembrane domain of IP_3R could be replaced with the transmembrane domain of RyR in chimeric proteins which maintained an ability to function as receptor channels [78].

The common distance (~70 Å) between the N-terminal regions and transmembrane domain may suggest that these proteins share a similar allosteric mechanism of regulating the channel activity through events such as Ca^{2+}/ligand-induced conformational changes in the NT/ABC regions. Since the 'arm'-motifs of RyR-A and IP_3R-SD reside in these inner core spaces, any conformational changes and/or alternate splicing in this region, known to occur in IP_3R for example, are likely to have significant impact on the allosteric regulation of these Ca^{2+} release channels.

3.3. Disease-associated mutations in three-dimensional structures of RyRs

The crystal structure of the RyR1-ABC and the docking model of RyR1-ABC in the cryo-EM map have provided new insights into the effect of disease-associated mutations on the three-dimensional structures of RyRs [86]. The mapping of fifty-six disease-associated mutations (*i.e.* 33 mutations from RyR1 and 23 mutations from RyR2) onto the RyR1-ABC structure clearly shows that most of these mutations are positioned at the intra-subunit interfaces within the ABC domain or inter-subunit interfaces between adjacent ABC subunits in the docking model (Fig. 1H).

The inter-subunit interface between domain A comprised mainly of residues from the HS loop and domain B comprised mainly of residues from two flexible loops is the site of 19 disease-associated mutations. Another inter-subunit interface that is concentrated with mutations lies between domain A and electron-dense columns which extend towards the transmembrane domains [86]. Considering the high frequency of disease-associated mutations found at the inter- and intra-subunit interfaces, destabilization of these interfaces likely facilitates the movement of individual domains, resulting in dysfunctional open probabilities. Indeed, docking studies of RyR1-ABC into the open- and closed-state cryo-EM maps of RyR have revealed that the inter-subunit distance between domain A and domain B of neighboring subunits increases by ~7 Å in the open state compared to that in the closed state [87,101]. The conformational changes within N-terminal regions of RyR between open and closed states are also supported by fluorescence resonance energy transfer (FRET) analysis [102]. These data imply that widening of inter-subunit gaps and perturbation of inter-subunit contacts are associated with channel opening.

Crystal structures of disease-associated mutants of RyR1-ABC have also revealed that buried mutations can have propagative effects on inter-subunit interfaces [87]. For example, mutations at buried positions L14R and G249R (*i.e.* PDB codes 4I7I and 4I1E, respectively) seem to alter the inter-subunit interfaces by displacing the neighboring side chains in loop regions *via* the introduction of bulky charged side chains (Fig. 3A). Perturbations of RyR1-ABC structures by salt-bridge mutations at the domain A:C intra-subunit interface (*i.e.* R45C, D61N and R402G; PDB codes 4I6I, 4I3N and 4I37, respectively) also cause inter-subunit orientation changes. Thus, a single mutation can result in long-range structural changes which affect inter-subunit interfaces (Fig. 3B). Lastly, some mutations at the intra-subunit A–B–C interface (*i.e.* C36R, V219I and I404M; PDB codes 4I0Y, 4I8M and 4I2S, respectively) do not induce large structural changes, but lower the thermal stabilities, suggesting that at any given time a larger fraction of unfolded states would be accessed by these mutants. Together, these results suggest that direct or indirect perturbations of inter-subunit interfaces between RyR1-ABCs are common mechanisms of dysfunction for this class of receptor Ca^{2+} channels.

Recently, crystal structures of the wild-type RyR2-ABC (*i.e.* residues 1–547 of mouse RyR2; PDB code 4L4H) and R420Q mutated RyR2-ABC (*i.e.* PDB code 4L4I) which have been linked to CPVT were solved [103,104]. The overall domain orientation of RyR2-ABC is similar to that of RyR1-ABC, but the pattern of ionic pair stabilizing the structure is different. RyR1-ABC has an ionic pair network formed by four residues (*i.e.* R283–D61–R402–E40). In RyR2-ABC, however, only the R298–D61 ionic pair is maintained, and a chloride ion interacts with the three charged residues R420, R298 and R276. The R420Q RyR2-ABC structure shows no density for this chloride ion, thus breaking the charged link between domains B and C (Fig. 3C) and causing domain reorientation between domains A/B and C.

Eleven disease-associated mutations are found in the structure of the RyR1 phosphorylation domain, and they are divided into three groups [89]. The seven mutations in the first group are located near the S2843 phosphorylation site (*i.e.* R2840W, S2843P, E2764K, S2776M, S2776F, L2785V and T2787S). The second group contains three mutations which are located on the opposite face of the first group (*i.e.* R2939S, R2939K and E2880K), and the last group contains the L2867G mutation which targets a buried residue. Most mutants have a minimal effect on the thermal stability except for L2867G, which also failed to crystallize. The structural integrity of the several mutants of which crystal structures were solved remains intact [89]. The crystal structures of those mutants reveal that disease mutations can alter the surface charge (*i.e.* E2764K, PDB code 4ETT), disrupt the hydrogen bond network, induce loop rearrangement (*i.e.* S2776M, PDB code 4ESU), and disrupt salt bridges, hydrogen bonds, and van der Waals contacts, resulting in increased flexibility (*i.e.* R2939S, PDB code 4ETU) (Fig. 3D).

More recently, the relationships between disease-associated mutations of RyR1 and calmodulin (CaM) binding were investigated by isothermal titration calorimetry (ITC) [105]. Several genetic diseases are often related with an increasing sensitivity of RyRs to Ca^{2+}, and the sensitivity of RyRs can be fine-tuned by many accessory proteins, such as CaM [106]. Two disease mutations are located on the third CaM-binding domains of RyR1 termed CaMBD3 (*i.e.* residues 4295–4325). The R4325D mutation is associated with CCD and multiminicore disease and a duplication mutation of the Leu-Arg-Arg sequence (*i.e.* L4319–R4320–R4321) has been linked to MH by increasing levels of creatine kinase [107]. Both these disease-associated mutations in CaMBD3 of RyR1 directly affect the binding between RyR1 and CaM in both Ca^{2+}-free and Ca^{2+}-bound states.

4. NMR spectroscopy of IP_3R and RyRs

While the crystal structures have provided most of the static structural pictures of the enormous cytosolic domains within RyRs and

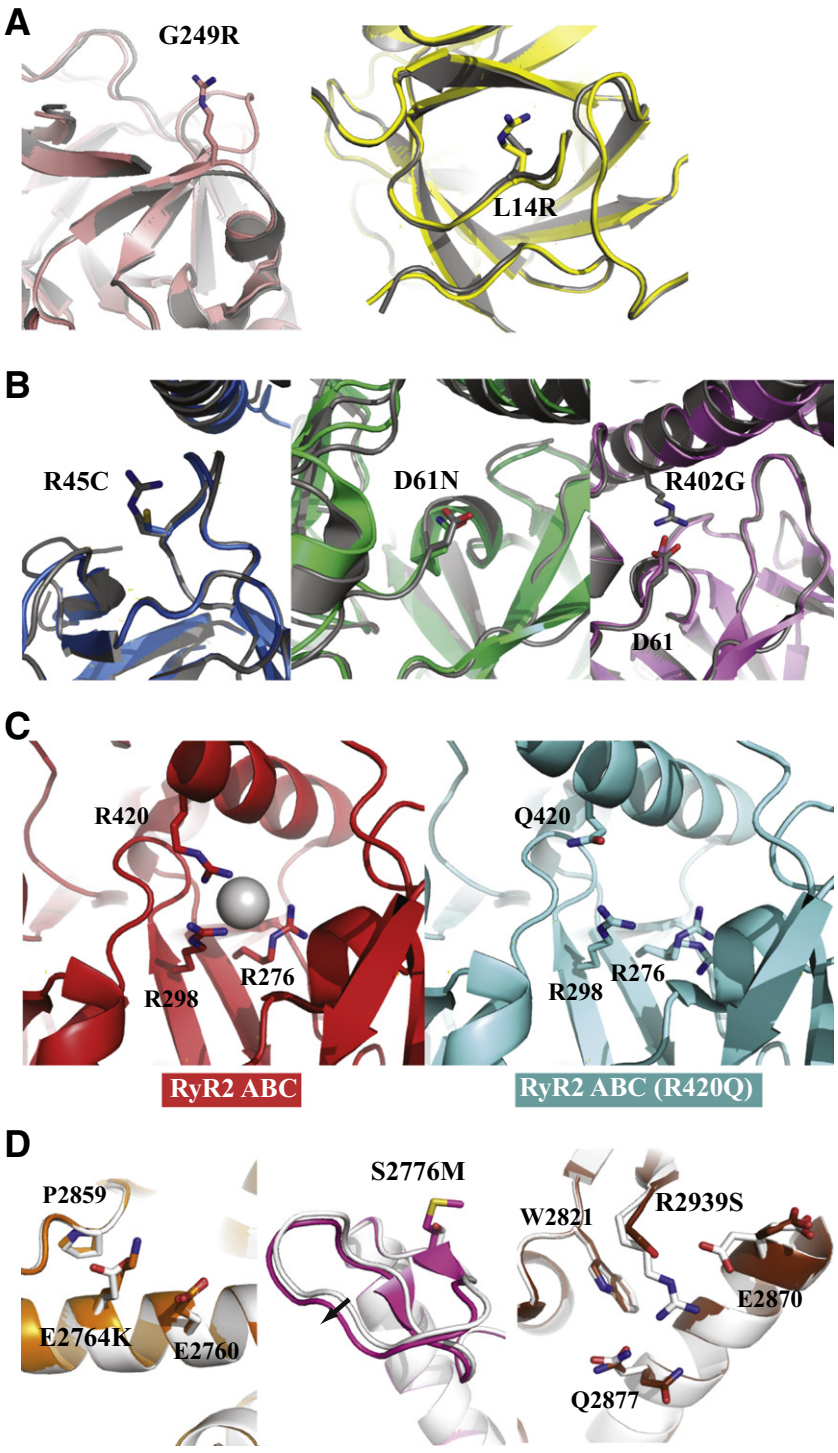

Fig. 3. Disease-associated mutations in the high-resolution structures of RyRs. Superposition of the wild-type RyR1-ABC structure (gray, PDB code 2XOA) and mutant structures for (A, B). Crystal structures of RyR1-ABC mutants at buried positions (A) and mutants affecting inter-domain ionic pairs (B) are shown, and the mutated residues are depicted as sticks. Each mutant structure is colored light pink (G249R, PDB code 4I1E), yellow (L14R, PDB code 4I7I), blue (R45C, PDB code 4I6I), light green (D61N, PDB code 4I3N) and pink (R402G, PDB code 4I37), respectively. (C) Structures of wild-type RyR2-ABC (red, PDB code 4L4H) and R420Q mutant (cyan, PDB code 4L4I). The residues forming the ionic pair network *via* chloride ion (gray sphere) in wild-type and the corresponding residues in R420Q mutant are shown as sticks. (D) Crystal structure of the phosphorylation domain of RyR1 (white, PDB code 4ERT) is superposedon the structures of disease mutants (E2764K, orange, PDB code 4ETT; S2776M, magenta, PDB code 4ESU; R2939S, brown, PDB code 4ETU), respectively. The mutated residues and neighboring residues are depicted as sticks.

IP_3Rs (see above), solution NMR experiments have revealed dynamic information regarding the structures of these protein domains, vital for understanding how conformational changes mediate channel function in health and disease. This section reviews the available solution NMR data of the IP_3R and RyR N-terminal cytosolic domains.

4.1. Conformational exchange and binding in the IP_3R N-terminal domains

Even prior to the collective elucidation of the crystal structures of the IP_3R1 N-terminal domains (*i.e.* SD and IBC) revealing relative orientation changes with and without the IP_3 binding [78,79] (see Section 2),

solution NMR showed that conformational exchange exists in these domains, and remarkably, the structural switching is influenced by the presence of the IP_3 [108]. Specifically, solution NMR of the IBC in the absence of any ligand demonstrated $^{1}H–^{15}N$-HSQC spectral (*i.e.* reporting on the polypeptide backbone conformation) peak broadening and intensity heterogeneity; however, when IP_3 was added to the samples, the IBC spectrum dramatically improved as a single conformation was stabilized [108]. The solution NMR $^{1}H–^{15}N$-HSQC spectrum of the SD was in good agreement with a well-folded domain and did not change in response to IP_3. Nevertheless, NMR analysis of the full NT (*i.e.* SD together with the IBC) exhibited severe peak broadening both in the presence and absence of the IP_3 ligand, beyond what is expected for the increased size of the NT compared to the separate IBC and SD; moreover, this broadening is indicative of the presence of different conformational sub-states within the IP_3R1-NT irrespective of IP_3 levels [108]. Overall, this solution data showed that IP_3 binding shifts the conformational equilibrium of the IP_3R1-NTs towards a compacted state and that this cytosolic region is in a dynamic conformational exchange at all times.

The initial structural changes (*i.e.* closing of the clam-like IBC structure and SD rotation towards the IBC) are believed to trigger the allostery required for gating of the channel pore (see Section 2) [78]. Precisely how the gating works is still a matter of debate and requires more structural studies. Nonetheless, solution NMR experiments have provided a few possibilities for linking these initial structural changes to downstream gating. It was reported that Y167 of IP_3R1 (*i.e.* W168 in IP_3R3) in the SD is required for Ca^{2+} channel activity (see Section 2) [109]. Further, a C-terminal fragment of IP_3R1 corresponding to residues 2418–2749 was suggested to inter-molecularly interact (*i.e.* between adjacent subunits) with the NT of these receptors, thereby linking structural changes in the cytosolic domains with pore regulation in the transmembrane domains [110]. Additionally, mutations in the loop region between transmembrane segments 4 and 5 (*i.e.* M4–M5 region, residues 2418–2437) have been shown to abolish channel activity [111]. Solution, NMR titrations of the IP_3R3-SD with two M4–M5 linker peptides covering residues 2356–2365 (*i.e.* 2418–2437 in IP_3R1) showed peak broadening indicative of relatively transient binding; however, among the three residues which showed >20% peak intensity differences (*i.e.* E19, W168 and S218) in the presence of the peptides was W168 (*i.e.* Y167 in IP_3R1), previously shown to be essential for channel activation [81,109]. Taken together, these solution data suggest that structural changes in the IP_3R-SD may be linked to channel gating interactions with the M4–M5 transmembrane region. Further structural work is required to determine the relevance of these weak interactions and a fuller picture by which N-terminal allostery is linked to transmembrane gating of the pore.

4.2. Regulation of IP_3R1-NTs by CaBP1

It has been well established that IP_3R activity can be positively and negatively modulated by Ca^{2+} levels [9,112–114]. In addition to the large body of evidence demonstrating activity modulation by the promiscuous and ubiquitous calmodulin [115–126], Ca^{2+} binding protein-1 (CaBP1) can regulate these receptor channels [127,128]. Solution NMR experiments were successful at linking these observations by demonstrating that direct interactions between Ca^{2+}-bound CaBP1 and residues on the IP_3R1-NT (*i.e.* residues 1–587) take place [129]. Interestingly, the data showed that the CaBP1-binding site of IP_3R involves both the SD and the IBC since $^{1}H–^{15}N$-HSQC spectra of Ca^{2+}-CaBP1 failed to exhibit any perturbations in response to separate addition of unlabelled SD or IBC proteins [129]. Additionally, the NMR spectral changes were localized to the C-terminal domain of CaBP1, suggesting that the N-lobe does not interact with the IP_3R1-NT, and Ca^{2+}-free CaBP1 exhibited at least 10-fold less affinity compared to Ca^{2+}-loaded for the IP_3R1-NT, consistent with a vital role for cytosolic Ca^{2+} levels in mediating this binding [129]. More recently, using a clever approach of site-directed labeling of the IP_3R1-NT [*i.e.* rationalized from the recent full-length NT structures (see Section 2)] with paramagnetic spin tags, residues V101, L104 and V162 on the C-lobe of CaBP1 which showed broadened $^{1}H–^{13}C$-methyl resonances were found to interact with a hydrophobic cluster on the IBC-β [100]. While no residues of interaction were identified on the SD using this methodology, NMR-data-guided docking of the Ca^{2+}-bound CaBP1 C-lobe revealed a close apposition to the interface between the SD and the IBC, as originally suggested [100,129].

4.3. Effect of disease-associated mutations on RyR1-A conformation

The first crystal structure of the RyR1-A (*i.e.* residues 1–214) demonstrated that as many as 8 mutations associated with MH and CCD are localized on the HS loop between β8 and β9 of domain A; further, RyR2 disease mutations associated with cardiomyocyte arrhythmias and tachycardias also map to this HS-loop (see Section 2) [83,130, 131]. Solution NMR was used to probe the effect of disease-associated mutations on the HS-loop structure. It became apparent that for some mutants (*i.e.* R164C) very minimal structural perturbations occur within domain A, while other mutations (*i.e.* R178C) resulted in localized changes within the loop and surrounding region in the absence of any global structural or stability disruption [83]. Together, the data suggest that different RyR1 mutations may manifest disease through different mechanisms of channel dysfunction.

4.4. Elucidation of a dynamic hidden arm-domain helix in the RyR2-A

The arm region of RyR-A varies considerably among three types of RyRs. Compared to the IP_3R1-SD containing a helix–loop–helix arm domain, RyR1 and RyR3 have a deletion in the sequence responsible for fully constituting this motif, while the RyR2 homolog has a 12-residue insertion in this stretch more similar to the IP_3Rs (Fig. 4A and B). The RyR1-A and RyR1-ABC crystal structures exhibit low electron density in this arm domain region, indicative of the unstable structural fold [83,86]. Surprisingly, however, a crystal structure of the RyR2-A also shows relatively weak electron density in this region with no discernible secondary structure (Fig. 4C) [84]. Remarkably, three dimensional solution NMR data of a RyR2-A construct consisting of residues 10–224 revealed that, in fact, a previously unidentified α-helix is present between V95–T104 within the 12-residue insertion of RyR2-A, not observable in the crystal structure [132]. The NMR data-derived chemical shift index (CSI) of the RyR2-A construct showed that the structural motifs as well as their relative locations in solution are identical to those revealed by the RyR1-A, RyR1-ABC and RyR2-A crystal structures [83, 84, 86, 132]; however, a clear α-helix in the 95–104 residue stretch is also indicated by the CSI data [132].

The conservation of position and type of secondary structural element with available crystal structure data [84] taken together with the solution data facilitated the calculation of a crystal/NMR hybrid structure, which shows that the α2 arm helix, only observable by NMR, exhibits a higher backbone root mean square deviation (rmsd) compared to the rest of the structural elements (Fig. 4D) [132]. This higher rmsd is consistent with backbone relaxation measurements which indicate that the α2 helix undergoes fast internal motions on the ~ps–ns timescales (*i.e.* lower $^{15}N–\{^{1}H\}$ heteronuclear NOE and elevated R1) relative to the global fold of the domain; moreover, the N- and C-terminal sequences flanking the α2 helix appear primarily responsible for this increased mobility. The NMR data also revealed chemical exchange on a very slow timescale (*i.e.* ~ms–s) for many residues on the face of the RyR2-A crystal/NMR hybrid structure adjacent to the α2 helix, as peak doubling was apparent in the $^{1}H–^{15}N$-HSQC spectra indicating that those residues readily and stably access multiple conformations [132].

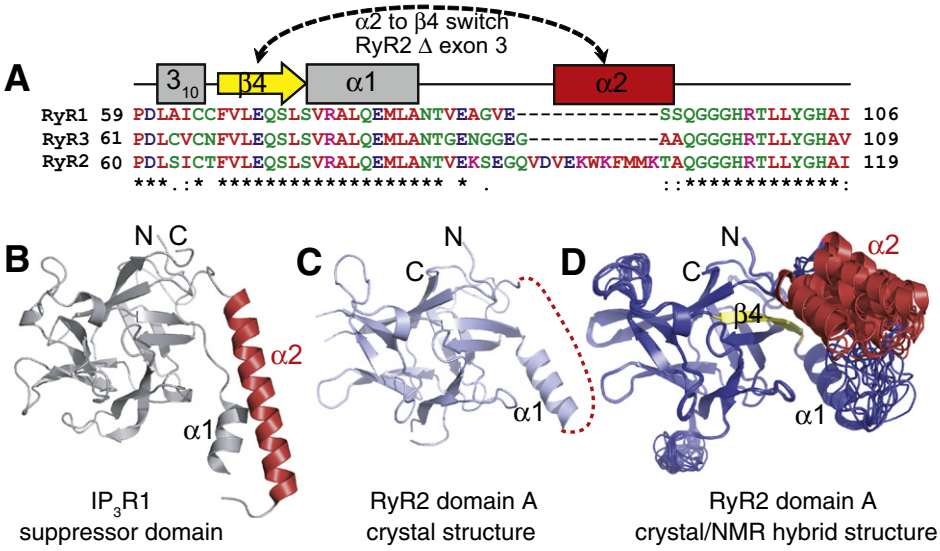

Fig. 4. Sequence alignment of the RyR human homologs and relative positions of the α2 helix in the IP_3R1-SD and the RyR2-A crystal and crystal/NMR hybrid structures. (A) Multi-sequence alignment of the human RyR1 (NCBI accession: P21817.3), RyR2 (Q92736.3) and RyR3 (Q15413.3) domain A regions that include the β4 strand, α1 and α2 helices. RyR1, RyR2 and RyR3 show a very high sequence identity in the region leading up to the 12-residue insertion that is specific to the RyR2 homolog as well as the region after the insertion. Fully, highly and partially conserved residues are indicated by '*', ':' and '.', respectively, below the amino acid sequences. The secondary structure elements revealed by the high resolution structures are indicated above the sequences with the β4 strand colored yellow and the α2 helix which is only NMR-visible colored red. The amino acid ranges are indicated at the left and right of each respective sequence. Alignment was done in ClustalW. (B) SD structure of IP_3R1 solved by X-ray crystallography. This structure (PDB code 1XZZ) shows the arm region composed of α1 and α2 relative to the position of the β-trefoil. The α2 helix, structurally conserved in the RyR2-A is colored red. (C) RyR2-A structure solved by X-ray crystallography. The α2 helix is not resolved in the RyR2-A crystal structure (PDB code 3IM5) due to the high mobility. The position of the polypeptide chain that makes up α2 relative to the β-trefoil and the α1 helix is shown with the red broken line. (D) RyR2-A structure solved using an X-ray crystallography/NMR hybrid approach (PDB code 2MC2). The α2 helix, visible only by NMR is colored red. The β4 strand which is deleted in the delta exon 3 mutant is colored yellow (see also Fig. 1G). The α2 helix rescues the β4 strand in the delta exon 3 mutant *via* a helix-to-strand structural transition.

4.5. Effect of disease-associated mutations on RyR2-A dynamics

A particularly remarkable structural transformation occurs in the RyR2-A harboring a heritable deletion mutation (*i.e.* delta exon 3) which causes VT [133]. The RyR2-A delta exon 3 mutant which carries an N57 to G91 deletion remains fully folded as a β-strand is inserted into the β-trefoil, thereby rescuing the overall fold (Figs. 1G and 4D) [85]. Solution NMR data showed that the dynamic α2 arm helix facilitates this switch, as CSI data convert from strong positive (*i.e.* α2-helix) to negative values (*i.e.* β4-strand) in the stretch of amino acids responsible for forming the α2 helix in the wild-type protein [132]. Analysis of the backbone dynamics of RyR2-A delta exon 3 suggests that the loops flanking the rescued β4 strand exhibit high mobility on a fast timescale in contrast to the β4 strand itself which is relatively immobile, consistent with data showing overall stabilization of delta exon 3 compared to wild-type [85,132].

Interestingly, three HS-loop mutants that cause heritable arrhythmia and tachycardia phenotypes (*i.e.* P164S, R169Q and R176Q) show only local structural perturbations confined to the immediate vicinity of the mutation, by NMR and crystal structure analyses; moreover, ^{15}N–{^1H} backbone dynamics measurements are consistent with these localized effects, as mobility parameters and peak doubling were all similar to the wild-type domain [132]. These data suggest that since the mutants have conserved overall fold, the dysfunction of the receptor must occur through perturbed interfaces involved in facilitating channel gating. Further structural and dynamics assessments are required to tease out the precise signaling dysfunctions caused by these mutations.

5. Concluding remarks

The currently available structural information has significantly advanced our understanding of the relationship between structure and function of Ca^{2+} release channels on the ER/SR membrane. Furthermore, the utilization of multiple techniques, including X-ray crystallography, NMR spectroscopy and EM, has produced a remarkable synergy in understanding the mechanisms of IP_3R and RyR function. For instance, the combination of X-ray crystallography and cryo-EM has enabled us to identify the location of the N-terminal region of RyR1 relative to the enormous fully-assembled tetrameric channel, thereby revealing the importance of inter-subunit interfaces and providing new insights into the effects of disease-associated mutations [86,87]. Notably, the docking models of IP_3R1-NT and RyR1-ABC in each cryo-EM map have also revealed structural and functional similarities between these two receptor channels [78]. Solution NMR spectroscopy has also provided important new structural information on these receptor channels, not observable by either X-ray crystallography or EM; further, dynamic properties of IP_3R and RyR domains in solution have also been elucidated by NMR.

Nevertheless, despite marked advances in the structural studies of IP_3Rs and RyRs in the past decade, the high-resolution data are limited only to the N-terminal regions of IP_3Rs and RyRs or the phosphorylation domain of RyRs. The currently unresolved domains containing the regulatory region and channel domains comprise the bulk of the channels (*i.e.* ~78% for IP_3R1 and ~85% for RyR1). In order to fully understand the integrated regulatory mechanisms of intracellular Ca^{2+} homeostasis by Ca^{2+} release channels, the structures of these remaining domains must be solved at high resolution. Further, these structures must be used to answer fundamental questions about IP_3R and RyR function. First, where is the bona fide Ca^{2+}-binding sites in IP_3R and RyR and how does Ca^{2+} binding regulate both IP_3R and RyR Ca^{2+} release activities in a bell-shaped manner? Although many researchers have intensively investigated the location and function of the Ca^{2+}-binding sites [134–137], ambiguity and uncertainty remain regarding the true Ca^{2+} binding sites. Second, how does the N-terminal domain allosterically regulate the channel domain in the activation mechanisms of IP_3R and RyR? In IP_3Rs, the link between structural changes within IP_3-binding N-terminal domain and the channel opening remains unknown. In RyRs, how do the disease-associated mutations in RyR isoforms perturb normal channel gating, thereby resulting in dysfunctional skeletal and cardiac muscle contraction? Third, how is IP_3R and RyR gating

distinctively modulated by other cellular signals such as phosphorylation, ATP binding, protein–protein interaction and oxidative stress? Elucidating the channel gating mechanisms of both channels in the context of molecular complexes will provide new insights into the versatility of Ca^{2+} signaling. A final question is why and how have the two distinct ER Ca^{2+} channels, IP_3R and RyR emerged in evolution? Recent genomic analyses have revealed the presence of putative IP_3Rs and RyRs in the unicellular eukaryotes [138–141]. Putative IP_3R homologs have been cloned and functionally characterized in the ciliate Paramecium and pathogenic unicellular parasites Trypanosomatids [142–146]. The phylogenetic relationship of IP_3Rs and RyRs in eukaryotes suggests that the divergence occurred along with or shortly before the emergence of multicellular organisms [147]. Further structural and functional studies of IP_3R/RyR homologs in lower eukaryotes will allow us to appreciate the rudimentary mechanisms of channel activation and modulation and deepen our understanding of the evolutionary aspect of the Ca^{2+} signaling tool kit.

Acknowledgements

This work was supported by Basic Science Research Program through the National Research Foundation (NRF) of Korea funded by the Ministry of Science, ICT & Future Planning (2012R1A1A1039738) (to M.-D. Seo) and by Canadian Institutes of Health Research and Heart and Stroke Foundation of Canada (to M.I.). This work was also supported by the Natural Sciences and Engineering Research Council of Canada (to P.B.S.).

References

[1] M.J. Berridge, Inositol trisphosphate and calcium signalling, Nature 361 (1993) 315–325.
[2] D.E. Clapham, Calcium signaling, Cell 80 (1995) 259–268.
[3] D.E. Clapham, Calcium signaling, Cell 131 (2007) 1047–1058.
[4] M.J. Berridge, M.D. Bootman, H.L. Roderick, Calcium signalling: dynamics, homeostasis and remodelling, Nat. Rev. Mol. Cell Biol. 4 (2003) 517–529.
[5] M.J. Berridge, P. Lipp, M.D. Bootman, The versatility and universality of calcium signalling, Nat. Rev. Mol. Cell Biol. 1 (2000) 11–21.
[6] J.K. Foskett, C. White, K.H. Cheung, D.O. Mak, Inositol trisphosphate receptor Ca^{2+} release channels, Physiol. Rev. 87 (2007) 593–658.
[7] J.T. Lanner, D.K. Georgiou, A.D. Joshi, S.L. Hamilton, Ryanodine receptors: structure, expression, molecular details, and function in calcium release, Cold Spring Harb. Perspect. Biol. 2 (2010) a003996.
[8] G. Meissner, Ryanodine activation and inhibition of the Ca^{2+} release channel of sarcoplasmic reticulum, J. Biol. Chem. 261 (1986) 6300–6306.
[9] I. Bezprozvanny, J. Watras, B.E. Ehrlich, Bell-shaped calcium-response curves of Ins (1,4,5) P3- and calcium-gated channels from endoplasmic reticulum of cerebellum, Nature 351 (1991) 751–754.
[10] H.L. Roderick, M.D. Bootman, Calcium influx: is Homer the missing link? Curr. Biol. 13 (2003) R976–R978.
[11] I. Bezprozvanny, The inositol 1,4,5-trisphosphate receptors, Cell Calcium 38 (2005) 261–272.
[12] L. Ottini, G. Marziali, A. Conti, A. Charlesworth, V. Sorrentino, Alpha and beta isoforms of ryanodine receptor from chicken skeletal muscle are the homologues of mammalian RyR1 and RyR3, Biochem. J. 315 (Pt 1) (1996) 207–216.
[13] H. Sugawara, M. Kurosaki, M. Takata, T. Kurosaki, Genetic evidence for involvement of type 1, type 2 and type 3 inositol 1,4,5-trisphosphate receptors in signal transduction through the B-cell antigen receptor, EMBO J. 16 (1997) 3078–3088.
[14] M.J. Berridge, Calcium hypothesis of Alzheimer's disease, Pflugers Arch. 459 (2010) 441–449.
[15] I. Bezprozvanny, Calcium signaling and neurodegenerative diseases, Trends Mol. Med. 15 (2009) 89–100.
[16] I. Bezprozvanny, Role of inositol 1,4,5-trisphosphate receptors in pathogenesis of Huntington's disease and spinocerebellar ataxias, Neurochem. Res. 36 (2011) 1186–1197.
[17] I. Bezprozvanny, M.P. Mattson, Neuronal calcium mishandling and the pathogenesis of Alzheimer's disease, Trends Neurosci. 31 (2008) 454–463.
[18] A. Fiorio Pla, D. Avanzato, L. Munaron, I.S. Ambudkar, Ion channels and transporters in cancer. 6. Vascularizing the tumor: TRP channels as molecular targets, Am. J. Physiol. Cell Physiol. 302 (2012) C9–C15.
[19] J.K. Foskett, Inositol trisphosphate receptor Ca^{2+} release channels in neurological diseases, Pflugers Arch. 460 (2010) 481–494.
[20] V. Lehen'kyi, G. Shapovalov, R. Skryma, N. Prevarskaya, Ion channnels and transporters in cancer. 5. Ion channels in control of cancer and cell apoptosis, Am. J. Physiol. Cell Physiol. 301 (2011) C1281–C1289.
[21] N. Prevarskaya, R. Skryma, Y. Shuba, Calcium in tumour metastasis: new roles for known actors, Nat. Rev. Cancer 11 (2011) 609–618.
[22] R. Rizzuto, P. Pinton, D. Ferrari, M. Chami, G. Szabadkai, P.J. Magalhaes, F. Di Virgilio, T. Pozzan, Calcium and apoptosis: facts and hypotheses, Oncogene 22 (2003) 8619–8627.
[23] H.L. Roderick, S.J. Cook, Ca^{2+} signalling checkpoints in cancer: remodelling Ca^{2+} for cancer cell proliferation and survival, Nat. Rev. Cancer 8 (2008) 361–375.
[24] J.F. Whitfield, Calcium signals and cancer, Crit. Rev. Oncog. 3 (1992) 55–90.
[25] J.M. Lee, F.M. Davis, S.J. Roberts-Thomson, G.R. Monteith, Ion channels and transporters in cancer. 4. Remodeling of Ca(2+) signaling in tumorigenesis: role of Ca(2+) transport, Am. J. Physiol. Cell Physiol. 301 (2011) C969–C976.
[26] G.R. Monteith, F.M. Davis, S.J. Roberts-Thomson, Calcium channels and pumps in cancer: changes and consequences, J. Biol. Chem. 287 (2012) 31666–31673.
[27] A.S. Dhillon, S. Hagan, O. Rath, W. Kolch, MAP kinase signalling pathways in cancer, Oncogene 26 (2007) 3279–3290.
[28] S.S. Kang, K.S. Han, B.M. Ku, Y.K. Lee, J. Hong, H.Y. Shin, A.G. Almonte, D.H. Woo, D.J. Brat, E.M. Hwang, S.H. Yoo, C.K. Chung, S.H. Park, S.H. Paek, E.J. Roh, S.J. Lee, J.Y. Park, S.F. Traynelis, C.J. Lee, Caffeine-mediated inhibition of calcium release channel inositol 1,4,5-trisphosphate receptor subtype 3 blocks glioblastoma invasion and extends survival, Cancer Res. 70 (2010) 1173–1183.
[29] K. Shibao, M.J. Fiedler, J. Nagata, N. Minagawa, K. Hirata, Y. Nakayama, Y. Iwakiri, M.H. Nathanson, K. Yamaguchi, The type III inositol 1,4,5-trisphosphate receptor is associated with aggressiveness of colorectal carcinoma, Cell Calcium 48 (2010) 315–323.
[30] C. Li, X. Wang, H. Vais, C.B. Thompson, J.K. Foskett, C. White, Apoptosis regulation by Bcl-x(L) modulation of mammalian inositol 1,4,5-trisphosphate receptor channel isoform gating, Proc. Natl. Acad. Sci. U. S. A. 104 (2007) 12565–12570.
[31] Y.P. Rong, A.S. Aromolaran, G. Bultynck, F. Zhong, X. Li, K. McColl, S. Matsuyama, S. Herlitze, H.L. Roderick, M.D. Bootman, G.A. Mignery, J.B. Parys, H. De Smedt, C.W. Distelhorst, Targeting Bcl-2–IP3 receptor interaction to reverse Bcl-2's inhibition of apoptotic calcium signals, Mol. Cell 31 (2008) 255–265.
[32] Y.P. Rong, G. Bultynck, A.S. Aromolaran, F. Zhong, J.B. Parys, H. De Smedt, G.A. Mignery, H.L. Roderick, M.D. Bootman, C.W. Distelhorst, The BH4 domain of Bcl-2 inhibits ER calcium release and apoptosis by binding the regulatory and coupling domain of the IP3 receptor, Proc. Natl. Acad. Sci. U. S. A. 106 (2009) 14397–14402.
[33] C. White, C. Li, J. Yang, N.B. Petrenko, M. Madesh, C.B. Thompson, J.K. Foskett, The endoplasmic reticulum gateway to apoptosis by Bcl-x(L) modulation of the InsP3R, Nat. Cell Biol. 7 (2005) 1021–1028.
[34] J. Downward, Targeting RAS signalling pathways in cancer therapy, Nat. Rev. Cancer 3 (2003) 11–22.
[35] C. Pierro, S.J. Cook, T.C. Foets, M.D. Bootman, H.L. Roderick, Oncogenic K-Ras suppresses IP3-dependent Ca^{2+} release through remodeling of IP3Rs isoform composition and ER luminal Ca^{2+} levels in colorectal cancer cell lines, J. Cell Sci. (2014).
[36] P.J. Sung, F.D. Tsai, H. Vais, H. Court, J. Yang, N. Fehrenbacher, J.K. Foskett, M.R. Philips, Phosphorylated K-Ras limits cell survival by blocking Bcl-xL sensitization of inositol trisphosphate receptors, Proc. Natl. Acad. Sci. U. S. A. 110 (2013) 20593–20598.
[37] R. Etcheberrigaray, N. Hirashima, L. Nee, J. Prince, S. Govoni, M. Racchi, R.E. Tanzi, D.L. Alkon, Calcium responses in fibroblasts from asymptomatic members of Alzheimer's disease families, Neurobiol. Dis. 5 (1998) 37–45.
[38] E. Ito, K. Oka, R. Etcheberrigaray, T.J. Nelson, D.L. McPhie, B. Tofel-Grehl, G.E. Gibson, D.L. Alkon, Internal Ca^{2+} mobilization is altered in fibroblasts from patients with Alzheimer disease, Proc. Natl. Acad. Sci. U. S. A. 91 (1994) 534–538.
[39] G.E. Stutzmann, The pathogenesis of Alzheimers disease is it a lifelong "calciumopathy"? Neuroscientist 13 (2007) 546–559.
[40] G.E. Stutzmann, A. Caccamo, F.M. LaFerla, I. Parker, Dysregulated IP3 signaling in cortical neurons of knock-in mice expressing an Alzheimer's-linked mutation in presenilin 1 results in exaggerated Ca^{2+} signals and altered membrane excitability, J. Neurosci.: Off. J. Soc. Neurosci. 24 (2004) 508–513.
[41] O. Nelson, H. Tu, T. Lei, M. Bentahir, B. de Strooper, I. Bezprozvanny, Familial Alzheimer disease-linked mutations specifically disrupt Ca^{2+} leak function of presenilin 1, J. Clin. Invest. 117 (2007) 1230–1239.
[42] H. Tu, O. Nelson, A. Bezprozvanny, Z. Wang, S.F. Lee, Y.H. Hao, L. Serneels, B. De Strooper, G. Yu, I. Bezprozvanny, Presenilins form ER Ca^{2+} leak channels, a function disrupted by familial Alzheimer's disease-linked mutations, Cell 126 (2006) 981–993.
[43] H. Zhang, S. Sun, A. Herreman, B. De Strooper, I. Bezprozvanny, Role of presenilins in neuronal calcium homeostasis, J. Neurosci.: Off. J. Soc. Neurosci. 30 (2010) 8566–8580.
[44] K.H. Cheung, L. Mei, D.O. Mak, I. Hayashi, T. Iwatsubo, D.E. Kang, J.K. Foskett, Gain-of-function enhancement of IP3 receptor modal gating by familial Alzheimer's disease-linked presenilin mutants in human cells and mouse neurons, Sci. Signal. 3 (2010) ra22.
[45] K.H. Cheung, D. Shineman, M. Muller, C. Cardenas, L. Mei, J. Yang, T. Tomita, T. Iwatsubo, V.M. Lee, J.K. Foskett, Mechanism of Ca^{2+} disruption in Alzheimer's disease by presenilin regulation of InsP3 receptor channel gating, Neuron 58 (2008) 871–883.
[46] A novel gene containing a trinucleotide repeat that is expanded and unstable on Huntington's disease chromosomes. The Huntington's Disease Collaborative Research Group, Cell 72 (1993) 971–983.
[47] A.J. Tobin, E.R. Signer, Huntington's disease: the challenge for cell biologists, Trends Cell Biol. 10 (2000) 531–536.
[48] T.S. Tang, H. Tu, E.Y. Chan, A. Maximov, Z. Wang, C.L. Wellington, M.R. Hayden, I. Bezprozvanny, Huntingtin and huntingtin-associated protein 1 influence neuronal calcium signaling mediated by inositol-(1,4,5) triphosphate receptor type 1, Neuron 39 (2003) 227–239.

[49] L.S. Kaltenbach, E. Romero, R.R. Becklin, R. Chettier, R. Bell, A. Phansalkar, A. Strand, C. Torcassi, J. Savage, A. Hurlburt, G.H. Cha, L. Ukani, C.L. Chepanoske, Y. Zhen, S. Sahasrabudhe, J. Olson, C. Kurschner, L.M. Ellerby, J.M. Peltier, J. Botas, R.E. Hughes, Huntingtin interacting proteins are genetic modifiers of neurodegeneration, PLoS Genet. 3 (2007) e82.

[50] T. Higo, K. Hamada, C. Hisatsune, N. Nukina, T. Hashikawa, M. Hattori, T. Nakamura, K. Mikoshiba, Mechanism of ER stress-induced brain damage by IP(3) receptor, Neuron 68 (2010) 865–878.

[51] H. Takeshima, S. Nishimura, T. Matsumoto, H. Ishida, K. Kangawa, N. Minamino, H. Matsuo, M. Ueda, M. Hanaoka, T. Hirose, et al., Primary structure and expression from complementary DNA of skeletal muscle ryanodine receptor, Nature 339 (1989) 439–445.

[52] B.W. Brandom, M.G. Larach, M.S. Chen, M.C. Young, Complications associated with the administration of dantrolene 1987 to 2006: a report from the North American Malignant Hyperthermia Registry of the Malignant Hyperthermia Association of the United States, Anesth. Analg. 112 (2011) 1115–1123.

[53] W.J. Durham, P. Aracena-Parks, C. Long, A.E. Rossi, S.A. Goonasekera, S. Boncompagni, D.L. Galvan, C.P. Gilman, M.R. Baker, N. Shirokova, F. Protasi, R. Dirksen, S.L. Hamilton, RyR1 S-nitrosylation underlies environmental heat stroke and sudden death in Y522S RyR1 knockin mice, Cell 133 (2008) 53–65.

[54] J.H. Hwang, F. Zorzato, N.F. Clarke, S. Treves, Mapping domains and mutations on the skeletal muscle ryanodine receptor channel, Trends Mol. Med. 18 (2012) 644–657.

[55] K. Jurkat-Rott, T. McCarthy, F. Lehmann-Horn, Genetics and pathogenesis of malignant hyperthermia, Muscle Nerve 23 (2000) 4–17.

[56] G. Avila, R.T. Dirksen, Functional effects of central core disease mutations in the cytoplasmic region of the skeletal muscle ryanodine receptor, J. Gen. Physiol. 118 (2001) 277–290.

[57] H. Jungbluth, Central core disease, Orphanet J Rare Dis. 2 (2007) 25.

[58] R.L. Robinson, C. Brooks, S.L. Brown, F.R. Ellis, P.J. Halsall, R.J. Quinnell, M.A. Shaw, P.M. Hopkins, RYR1 mutations causing central core disease are associated with more severe malignant hyperthermia in vitro contracture test phenotypes, Hum. Mutat. 20 (2002) 88–97.

[59] H. Jungbluth, Multi-minicore disease, Orphanet J Rare Dis. 2 (2007) 31.

[60] F. Van Petegem, Ryanodine receptors: structure and function, J. Biol. Chem. 287 (2012) 31624–31632.

[61] J.F. Capacchione, S.M. Muldoon, The relationship between exertional heat illness, exertional rhabdomyolysis, and malignant hyperthermia, Anesth. Analg. 109 (2009) 1065–1069.

[62] K. Paul-Pletzer, T. Yamamoto, M.B. Bhat, J. Ma, N. Ikemoto, L.S. Jimenez, H. Morimoto, P.G. Williams, J. Parness, Identification of a dantrolene-binding sequence on the skeletal muscle ryanodine receptor, J. Biol. Chem. 277 (2002) 34918–34923.

[63] F. Zhao, P. Li, S.R. Chen, C.F. Louis, B.R. Fruen, Dantrolene inhibition of ryanodine receptor Ca^{2+} release channels. Molecular mechanism and isoform selectivity, J. Biol. Chem. 276 (2001) 13810–13816.

[64] P. Szentesi, C. Collet, S. Sarkozi, C. Szegedi, I. Jona, V. Jacquemond, L. Kovacs, L. Csernoch, Effects of dantrolene on steps of excitation–contraction coupling in mammalian skeletal muscle fibers, J. Gen. Physiol. 118 (2001) 355–375.

[65] K. Otsu, H.F. Willard, V.K. Khanna, F. Zorzato, N.M. Green, D.H. MacLennan, Molecular cloning of cDNA encoding the Ca^{2+} release channel (ryanodine receptor) of rabbit cardiac muscle sarcoplasmic reticulum, J. Biol. Chem. 265 (1990) 13472–13483.

[66] J. Nakai, T. Imagawa, Y. Hakamat, M. Shigekawa, H. Takeshima, S. Numa, Primary structure and functional expression from cDNA of the cardiac ryanodine receptor/calcium release channel, FEBS Lett. 271 (1990) 169–177.

[67] P.J. Laitinen, K.M. Brown, K. Piippo, H. Swan, J.M. Devaney, B. Brahmbhatt, E.A. Donarum, M. Marino, N. Tiso, M. Viitasalo, L. Toivonen, D.A. Stephan, K. Kontula, Mutations of the cardiac ryanodine receptor (RyR2) gene in familial polymorphic ventricular tachycardia, Circulation 103 (2001) 485–490.

[68] S.G. Priori, S.R. Chen, Inherited dysfunction of sarcoplasmic reticulum Ca^{2+} handling and arrhythmogenesis, Circ. Res. 108 (2011) 871–883.

[69] D.H. MacLennan, S.R. Chen, Store overload-induced Ca^{2+} release as a triggering mechanism for CPVT and MH episodes caused by mutations in RYR and CASQ genes, J. Physiol. 587 (2009) 3113–3115.

[70] W. Chen, R. Wang, B. Chen, X. Zhong, H. Kong, Y. Bai, Q. Zhou, C. Xie, J. Zhang, A. Guo, X. Tian, P.P. Jones, M.L. O'Mara, Y. Liu, T. Mi, L. Zhang, J. Bolstad, L. Semeniuk, H. Cheng, J. Zhang, J. Chen, D.P. Tieleman, A.M. Gillis, H.J. Duff, M. Fill, L.S. Song, S.R. Chen, The ryanodine receptor store-sensing gate controls Ca^{2+} waves and Ca^{2+}-triggered arrhythmias, Nat. Med. 20 (2014) 184–192.

[71] N. Liu, B. Colombi, M. Memmi, S. Zissimopoulos, N. Rizzi, S. Negri, M. Imbriani, C. Napolitano, F.A. Lai, S.G. Priori, Arrhythmogenesis in catecholaminergic polymorphic ventricular tachycardia: insights from a RyR2 R4496C knock-in mouse model, Circ. Res. 99 (2006) 292–298.

[72] H. Watanabe, N. Chopra, D. Laver, H.S. Hwang, S.S. Davies, D.E. Roach, H.J. Duff, D.M. Roden, A.A. Wilde, B.C. Knollmann, Flecainide prevents catecholaminergic polymorphic ventricular tachycardia in mice and humans, Nat. Med. 15 (2009) 380–383.

[73] F.A. Hilliard, D.S. Steele, D. Laver, Z. Yang, S.J. Le Marchand, N. Chopra, D.W. Piston, S. Huke, B.C. Knollmann, Flecainide inhibits arrhythmogenic Ca^{2+} waves by open state block of ryanodine receptor Ca^{2+} release channels and reduction of Ca^{2+} spark mass, J Mol. Cell Cardiol. 48 (2010) 293–301.

[74] J. Liu, C. Supnet, S. Sun, H. Zhang, L. Good, E. Popugaeva, I. Bezprozvanny, The role of ryanodine receptor type 3 in a mouse model of Alzheimer disease, Channels 8 (2014).

[75] A.M. Bruno, J.Y. Huang, D.A. Bennett, R.A. Marr, M.L. Hastings, G.E. Stutzmann, Altered ryanodine receptor expression in mild cognitive impairment and Alzheimer's disease, Neurobiol. Aging 33 (1001) (2012) e1001–e1006.

[76] I. Bosanac, J.R. Alattia, T.K. Mal, J. Chan, S. Talarico, F.K. Tong, K.I. Tong, F. Yoshikawa, T. Furuichi, M. Iwai, T. Michikawa, K. Mikoshiba, M. Ikura, Structure of the inositol 1,4,5-trisphosphate receptor binding core in complex with its ligand, Nature 420 (2002) 696–700.

[77] I. Bosanac, H. Yamazaki, T. Matsu-Ura, T. Michikawa, K. Mikoshiba, M. Ikura, Crystal structure of the ligand binding suppressor domain of type 1 inositol 1,4,5-trisphosphate receptor, Mol. Cell 17 (2005) 193–203.

[78] M.D. Seo, S. Velamakanni, N. Ishiyama, P.B. Stathopulos, A.M. Rossi, S.A. Khan, P. Dale, C. Li, J.B. Ames, M. Ikura, C.W. Taylor, Structural and functional conservation of key domains in InsP3 and ryanodine receptors, Nature 483 (2012) 108–112.

[79] C.C. Lin, K. Baek, Z. Lu, Apo and InsP-bound crystal structures of the ligand-binding domain of an InsP receptor, Nat. Struct. Mol. Biol. 18 (2011) 1172–1174.

[80] F. Yoshikawa, M. Morita, T. Monkawa, T. Michikawa, T. Furuichi, K. Mikoshiba, Mutational analysis of the ligand binding site of the inositol 1,4,5-trisphosphate receptor, J. Biol. Chem. 271 (1996) 18277–18284.

[81] J. Chan, H. Yamazaki, N. Ishiyama, M.-D. Seo, T.K. Mal, T. Michikawa, K. Mikoshiba, M. Ikura, Structural studies of inositol 1,4,5-trisphosphate receptor: coupling ligand binding to channel gating, J. Biol. Chem. 285 (2010) 36092–36099.

[82] M. Iwai, T. Michikawa, I. Bosanac, M. Ikura, K. Mikoshiba, Molecular basis of the isoform-specific ligand-binding affinity of inositol 1,4,5-trisphosphate receptors, J. Biol. Chem. 282 (2007) 12755–12764.

[83] F.J. Amador, S. Liu, N. Ishiyama, M.J. Plevin, A. Wilson, D.H. MacLennan, M. Ikura, Crystal structure of type I ryanodine receptor amino-terminal beta-trefoil domain reveals a disease-associated mutation "hot spot" loop, Proc. Natl. Acad. Sci. U. S. A. 106 (2009) 11040–11044.

[84] P.A. Lobo, F. Van Petegem, Crystal structures of the N-terminal domains of cardiac and skeletal muscle ryanodine receptors: insights into disease mutations, Structure 17 (2009) 1505–1514.

[85] P.A. Lobo, L. Kimlicka, C.C. Tung, F. Van Petegem, The deletion of exon 3 in the cardiac ryanodine receptor is rescued by beta strand switching, Structure 19 (2011) 790–798.

[86] C.C. Tung, P.A. Lobo, L. Kimlicka, F. Van Petegem, The amino-terminal disease hotspot of ryanodine receptors forms a cytoplasmic vestibule, Nature 468 (2010) 585–588.

[87] L. Kimlicka, K. Lau, C.C. Tung, F. Van Petegem, Disease mutations in the ryanodine receptor N-terminal region couple to a mobile intersubunit interface, Nat. Commun. 4 (2013) 1506.

[88] P. Sharma, N. Ishiyama, U. Nair, W. Li, A. Dong, T. Miyake, A. Wilson, T. Ryan, D.H. MacLennan, T. Kislinger, M. Ikura, S. Dhe-Paganon, A.O. Gramolini, Structural determination of the phosphorylation domain of the ryanodine receptor, FEBS J. 279 (2012) 3952–3964.

[89] Z. Yuchi, K. Lau, F. Van Petegem, Disease mutations in the ryanodine receptor central region: crystal structures of a phosphorylation hot spot domain, Structure 20 (2012) 1201–1211.

[90] G.A. Mignery, C.L. Newton, B.T. Archer, T.C. Südhof, Structure and expression of the rat inositol 1,4,5-trisphosphate receptor, J. Biol. Chem. 265 (1990) 12679–12685.

[91] J.S. Smith, T. Imagawa, J. Ma, M. Fill, K.P. Campbell, R. Coronado, Purified ryanodine receptor from rabbit skeletal muscle is the calcium-release channel of sarcoplasmic reticulum, J. Gen. Physiol. 92 (1988) 1–26.

[92] S.J. Ludtke, I.I. Serysheva, S.L. Hamilton, W. Chiu, The pore structure of the closed RyR1 channel, Structure 13 (2005) 1203–1211.

[93] M. Samsó, T. Wagenknecht, P.D. Allen, Internal structure and visualization of transmembrane domains of the RyR1 calcium release channel by cryo-EM, Nat. Struct. Mol. Biol. 12 (2005) 539–544.

[94] S.J. Ludtke, I.I. Serysheva, Single-particle Cryo-EM of calcium release channels: structural validation, Curr. Opin. Struct. Biol. 23 (2013) 755–762.

[95] S.J. Ludtke, T.P. Tran, Q.T. Ngo, V.Y. Moiseenkova-Bell, W. Chiu, I.I. Serysheva, Flexible architecture of IP(3)R1 by Cryo-EM, Structure 19 (2011) 1192–1199.

[96] S.C. Murray, J. Flanagan, O.B. Popova, W. Chiu, S.J. Ludtke, I.I. Serysheva, Validation of cryo-EM structure of IP_3R1 channel, Structure 21 (2013) 900–909.

[97] W. Wriggers, S. Birmanns, Using situs for flexible and rigid-body fitting of multiresolution single-molecule data, J. Struct. Biol. 133 (2001) 193–202.

[98] S. Zissimopoulos, C. Viero, M. Seidel, B. Cumbes, J. White, I. Cheung, R. Stewart, L.H. Jeyakumar, S. Fleischer, S. Mukherjee, N.L. Thomas, A.J. Williams, F.A. Lai, N-terminus oligomerization regulates the function of cardiac ryanodine receptors, J. Cell Sci. 126 (2013) 5042–5051.

[99] S. Zissimopoulos, J. Marsh, L. Stannard, M. Seidel, F.A. Lai, N-terminus oligomerization is conserved in intracellular calcium release channels, Biochem. J. 459 (2014) 265–273.

[100] C. Li, M. Enomoto, A.M. Rossi, M.D. Seo, T. Rahman, P.B. Stathopulos, C.W. Taylor, M. Ikura, J.B. Ames, CaBP1, a neuronal Ca^{2+} sensor protein, inhibits inositol trisphosphate receptors by clamping intersubunit interactions, Proc. Natl. Acad. Sci. U. S. A. 110 (2013) 8507–8512.

[101] M. Samso, W. Feng, I.N. Pessah, P.D. Allen, Coordinated movement of cytoplasmic and transmembrane domains of RyR1 upon gating, PLoS Biol. 7 (2009) e85.

[102] X. Zhong, Y. Liu, L. Zhu, X. Meng, R. Wang, F. Van Petegem, T. Wagenknecht, S.R. Chen, Z. Liu, Conformational dynamics inside amino-terminal disease hotspot of ryanodine receptor, Structure 21 (2013) 2051–2060.

[103] L. Kimlicka, C.C. Tung, A.C. Carlsson, P.A. Lobo, Z. Yuchi, F. Van Petegem, The cardiac ryanodine receptor N-terminal region contains an anion binding site that is targeted by disease mutations, Structure 21 (2013) 1440–1449.

[104] A. Medeiros-Domingo, Z.A. Bhuiyan, D.J. Tester, N. Hofman, H. Bikker, J.P. van Tintelen, M.M. Mannens, A.A. Wilde, M.J. Ackerman, The RYR2-encoded ryanodine receptor/calcium release channel in patients diagnosed previously with either catecholaminergic polymorphic ventricular tachycardia or genotype negative, exercise-induced long

QT syndrome: a comprehensive open reading frame mutational analysis, J. Am. Coll. Cardiol. 54 (2009) 2065–2074.
[105] K. Lau, M.M. Chan, F. Van Petegem, Lobe-specific calmodulin binding to different ryanodine receptor isoforms, Biochemistry 53 (2014) 932–946.
[106] M. Nyegaard, M.T. Overgaard, M.T. Sondergaard, M. Vranas, E.R. Behr, L.L. Hildebrandt, J. Lund, P.L. Hedley, A.J. Camm, G. Wettrell, I. Fosdal, M. Christiansen, A.D. Borglum, Mutations in calmodulin cause ventricular tachycardia and sudden cardiac death, Am. J. Hum. Genet. 91 (2012) 703–712.
[107] M.C. Ibarra, S. Wu, K. Murayama, N. Minami, Y. Ichihara, H. Kikuchi, S. Noguchi, Y.K. Hayashi, R. Ochiai, I. Nishino, Malignant hyperthermia in Japan: mutation screening of the entire ryanodine receptor type 1 gene coding region by direct sequencing, Anesthesiology 104 (2006) 1146–1154.
[108] J. Chan, A.E. Whitten, C.M. Jeffries, I. Bosanac, T.K. Mal, J. Ito, H. Porumb, T. Michikawa, K. Mikoshiba, J. Trewhella, M. Ikura, Ligand-induced conformational changes via flexible linkers in the amino-terminal region of the inositol 1,4,5-trisphosphate receptor, J. Mol. Biol. 373 (2007) 1269–1280.
[109] H. Yamazaki, J. Chan, M. Ikura, T. Michikawa, K. Mikoshiba, Tyr-167/Trp-168 in type 1/3 inositol 1,4,5-trisphosphate receptor mediates functional coupling between ligand binding and channel opening, J. Biol. Chem. 285 (2010) 36081–36091.
[110] D. Boehning, S.K. Joseph, Direct association of ligand-binding and pore domains in homo- and heterotetrameric inositol 1,4,5-trisphosphate receptors, EMBO J. 19 (2000) 5450–5459.
[111] Z.T. Schug, S.K. Joseph, The role of the S4–S5 linker and C-terminal tail in inositol 1,4,5-trisphosphate receptor function, J. Biol. Chem. 281 (2006) 24431–24440.
[112] E.A. Finch, T.J. Turner, S.M. Goldin, Calcium as a coagonist of inositol 1,4,5-trisphosphate-induced calcium release, Science 252 (1991) 443–446.
[113] M. Iino, Biphasic Ca^{2+} dependence of inositol 1,4,5-trisphosphate-induced Ca release in smooth muscle cells of the guinea pig taenia caeci, J. Gen. Physiol. 95 (1990) 1103–1122.
[114] C.W. Taylor, A.J. Laude, IP3 receptors and their regulation by calmodulin and cytosolic Ca^{2+}, Cell Calcium 32 (2002) 321–334.
[115] X. Zhang, S.K. Joseph, Effect of mutation of a calmodulin binding site on Ca^{2+} regulation of inositol trisphosphate receptors, Biochem. J. 360 (2001) 395–400.
[116] M. Yamada, A. Miyawaki, K. Saito, T. Nakajima, M. Yamamoto-Hino, Y. Ryo, T. Furuichi, K. Mikoshiba, The calmodulin-binding domain in the mouse type 1 inositol 1,4,5-trisphosphate receptor, Biochem. J. 308 (Pt 1) (1995) 83–88.
[117] Y. Sun, C.W. Taylor, A calmodulin antagonist reveals a calmodulin-independent interdomain interaction essential for activation of inositol 1,4,5-trisphosphate receptors, Biochem. J. 416 (2008) 243–253.
[118] Y. Sun, A.M. Rossi, T. Rahman, C.W. Taylor, Activation of IP3 receptors requires an endogenous 1-8-14 calmodulin-binding motif, Biochem. J. 449 (2013) 39–49.
[119] H. Sipma, P. De Smet, I. Sienaert, S. Vanlingen, L. Missiaen, J.B. Parys, H. De Smedt, Modulation of inositol 1,4,5-trisphosphate binding to the recombinant ligand-binding site of the type-1 inositol 1,4, 5-trisphosphate receptor by Ca^{2+} and calmodulin, J. Biol. Chem. 274 (1999) 12157–12162.
[120] I. Sienaert, N. Nadif Kasri, S. Vanlingen, J.B. Parys, G. Callewaert, L. Missiaen, H. de Smedt, Localization and function of a calmodulin–apocalmodulin-binding domain in the N-terminal part of the type 1 inositol 1,4,5-trisphosphate receptor, Biochem. J. 365 (2002) 269–277.
[121] D.O. Mak, S.M. McBride, N.B. Petrenko, J.K. Foskett, Novel regulation of calcium inhibition of the inositol 1,4,5-trisphosphate receptor calcium-release channel, J. Gen. Physiol. 122 (2003) 569–581.
[122] N. Maeda, T. Kawasaki, S. Nakade, N. Yokota, T. Taguchi, M. Kasai, K. Mikoshiba, Structural and functional characterization of inositol 1,4,5-trisphosphate receptor channel from mouse cerebellum, J. Biol. Chem. 266 (1991) 1109–1116.
[123] C. Lin, J. Widjaja, S.K. Joseph, The interaction of calmodulin with alternatively spliced isoforms of the type-I inositol trisphosphate receptor, J. Biol. Chem. 275 (2000) 2305–2311.
[124] J. Hirota, T. Michikawa, T. Natsume, T. Furuichi, K. Mikoshiba, Calmodulin inhibits inositol 1,4,5-trisphosphate-induced calcium release through the purified and reconstituted inositol 1,4,5-trisphosphate receptor type 1, FEBS Lett. 456 (1999) 322–326.
[125] T.J. Cardy, C.W. Taylor, A novel role for calmodulin: Ca^{2+}-independent inhibition of type-1 inositol trisphosphate receptors, Biochem. J. 334 (Pt 2) (1998) 447–455.
[126] C.E. Adkins, S.A. Morris, H. De Smedt, I. Sienaert, K. Torok, C.W. Taylor, Ca^{2+}-calmodulin inhibits Ca^{2+} release mediated by type-1, -2 and -3 inositol trisphosphate receptors, Biochem. J. 345 (Pt 2) (2000) 357–363.
[127] N.N. Kasri, A.M. Holmes, G. Bultynck, J.B. Parys, M.D. Bootman, K. Rietdorf, L. Missiaen, F. McDonald, H. De Smedt, S.J. Conway, A.B. Holmes, M.J. Berridge, H.L. Roderick, Regulation of InsP3 receptor activity by neuronal Ca^{2+}-binding proteins, EMBO J. 23 (2004) 312–321.
[128] J. Yang, S. McBride, D.O. Mak, N. Vardi, K. Palczewski, F. Haeseleer, J.K. Foskett, Identification of a family of calcium sensors as protein ligands of inositol trisphosphate receptor Ca(2+) release channels, Proc. Natl. Acad. Sci. U. S. A. 99 (2002) 7711–7716.
[129] C. Li, J. Chan, F. Haeseleer, K. Mikoshiba, K. Palczewski, M. Ikura, J.B. Ames, Structural insights into Ca^{2+}-dependent regulation of inositol 1,4,5-trisphosphate receptors by CaBP1, J. Biol. Chem. 284 (2009) 2472–2481.
[130] C.H. Hsueh, Y.C. Weng, C.Y. Chen, T.K. Lin, Y.H. Lin, L.P. Lai, J.L. Lin, A novel mutation (Arg169Gln) of the cardiac ryanodine receptor gene causing exercise-induced bidirectional ventricular tachycardia, Int. J. Cardiol. 108 (2006) 276–278.
[131] P.J. Kannankeril, B.M. Mitchell, S.A. Goonasekera, M.G. Chelu, W. Zhang, S. Sood, D.L. Kearney, C.I. Danila, M. De Biasi, X.H. Wehrens, R.G. Pautler, D.M. Roden, G.E. Taffet, R.T. Dirksen, M.E. Anderson, S.L. Hamilton, Mice with the R176Q cardiac ryanodine receptor mutation exhibit catecholamine-induced ventricular tachycardia and cardiomyopathy, Proc. Natl. Acad. Sci. U. S. A. 103 (2006) 12179–12184.
[132] F.J. Amador, L. Kimlicka, P.B. Stathopulos, G.M. Gasmi-Seabrook, D.H. Maclennan, F. Van Petegem, M. Ikura, Type 2 ryanodine receptor domain A contains a unique and dynamic alpha-helix that transitions to a beta-strand in a mutant linked with a heritable cardiomyopathy, J. Mol. Biol. 425 (2013) 4034–4046.
[133] Z.A. Bhuiyan, M.P. van den Berg, J.P. van Tintelen, M.T. Bink-Boelkens, A.C. Wiesfeld, M. Alders, A.V. Postma, I. van Langen, M.M. Mannens, A.A. Wilde, Expanding spectrum of human RYR2-related disease: new electrocardiographic, structural, and genetic features, Circulation 116 (2007) 1569–1576.
[134] I. Sienaert, H. De Smedt, J.B. Parys, L. Missiaen, S. Vanlingen, H. Sipma, R. Casteels, Characterization of a cytosolic and a luminal Ca^{2+} binding site in the type I inositol 1,4,5-trisphosphate receptor, J. Biol. Chem. 271 (1996) 27005–27012.
[135] I. Sienaert, L. Missiaen, H. De Smedt, J.B. Parys, H. Sipma, R. Casteels, Molecular and functional evidence for multiple Ca^{2+}-binding domains in the type 1 inositol 1,4,5-trisphosphate receptor, J. Biol. Chem. 272 (1997) 25899–25906.
[136] T. Miyakawa, A. Mizushima, K. Hirose, T. Yamazawa, I. Bezprozvanny, T. Kurosaki, M. Iino, Ca(2+)-sensor region of IP(3) receptor controls intracellular Ca(2+) signaling, EMBO J. 20 (2001) 1674–1680.
[137] H. Tu, E. Nosyreva, T. Miyakawa, Z. Wang, A. Mizushima, M. Iino, I. Bezprozvanny, Functional and biochemical analysis of the type 1 inositol (1,4,5)-trisphosphate receptor calcium sensor, Biophys. J. 85 (2003) 290–299.
[138] X. Cai, Unicellular Ca^{2+} signaling 'toolkit' at the origin of metazoa, Mol. Biol. Evol. 25 (2008) 1357–1361.
[139] X. Cai, D.E. Clapham, Ancestral Ca^{2+} signaling machinery in early animal and fungal evolution, Mol. Biol. Evol. 29 (2011) 91–100.
[140] D.L. Prole, C.W. Taylor, Identification of intracellular and plasma membrane calcium channel homologues in pathogenic parasites, PLoS ONE 6 (2011) e26218.
[141] R. Docampo, S.N. Moreno, H. Plattner, Intracellular calcium channels in protozoa, Eur. J. Pharmacol. 739C (2014) 4–18.
[142] E.M. Ladenburger, I. Korn, N. Kasielke, T. Wassmer, H. Plattner, An Ins(1,4,5)P3 receptor in Paramecium is associated with the osmoregulatory system, J. Cell Sci. 119 (2006) 3705–3717.
[143] E.M. Ladenburger, H. Plattner, Calcium-release channels in Paramecium. Genomic expansion, differential positioning and partial transcriptional elimination, PLoS ONE 6 (2011) e27111.
[144] M. Hashimoto, M. Enomoto, J. Morales, N. Kurebayashi, T. Sakurai, T. Hashimoto, T. Nara, K. Mikoshiba, Inositol 1,4,5-trisphosphate receptor regulates replication, differentiation, infectivity and virulence of the parasitic protist *Trypanosoma cruzi*, Mol. Microbiol. 87 (2013) 1133–1150.
[145] G. Huang, P.J. Bartlett, A.P. Thomas, S.N. Moreno, R. Docampo, Acidocalcisomes of *Trypanosoma brucei* have an inositol 1,4,5-trisphosphate receptor that is required for growth and infectivity, Proc. Natl. Acad. Sci. U. S. A. 110 (2013) 1887–1892.
[146] M. Hashimoto, T. Nara, H. Hirawake, J. Morales, M. Enomoto, K. Mikoshiba, Antisense oligonucleotides targeting parasite inositol 1,4,5-trisphosphate receptor inhibits mammalian host cell invasion by *Trypanosoma cruzi*, Sci. Rep. 4 (2014) 4231.
[147] P.B. Stathopulos, M.D. Seo, M. Enomoto, F.J. Amador, N. Ishiyama, M. Ikura, Themes and variations in ER/SR calcium release channels: structure and function, Physiology (Bethesda) 27 (2012) 331–342.